Journal of Solid State Chemistry 183 (2010) 2298–2304

Contents lists available at ScienceDirect

Journal of Solid State Chemistry

journal homepage: www.elsevier.com/locate/jssc

Two 3D network complexes of Y(III) and Ce(III) with 2-fold interpenetration and reversible desorption–adsorption behavior of lattice water

Wenjuan Chu [a], Yong He [a], Qinghuan Zhao [b], Yaoting Fan [a,*], Hongwei Hou [a]

[a] Department of Chemistry, Zhengzhou University, Zhengzhou, Henan 450052, PR China
[b] High-Tech Research Center, Henan Academy of Sciences, Henan 450003, PR China

ARTICLE INFO

Article history:
Received 11 May 2010
Received in revised form
26 July 2010
Accepted 27 July 2010
Available online 3 August 2010

Keywords:
1,2-bis[3-(1,2,4-triazolyl)-4-amino-5-carboxylmethylthio]ethane (H_2L)
3D network
Lanthanide (III) complexes
Crystal structure
Adsorption material

ABSTRACT

Two novel inorganic–organic 3D network, namely{$[Ln(L)_{1.5}(H_2O)_2]\cdot 5H_2O$}$n$ [Ln=Y (1), Ce (2)] $[Ln(L)_{1.5}(H_2O)_2]\cdot 5H_2O$ [Ln=Y (1), Ce (2)], have been prepared through the assembly of the ligand 1,2-bis[3-(1,2,4-triazolyl)-4-amino-5-carboxylmethylthio]ethane (H_2L) and lanthanide (III) salts under hydrothermal condition and structurally characterized by single-crystal X-ray diffractions. In complexes **1** and **2**, the L^{2-} anions adopt three different coordination fashions (bidentate chelate, bidentate bridging and bidentate chelate bridging) connecting *Ln*(III) ions via the oxygen atoms from carboxylate moieties. Both 1 and 2 exhibit 3D network structures with 2-fold interpenetration. Interestingly, the reversible desorption–adsorption behavior of lattice water is significantly observed in the two compounds. The result shows their potential application as late-model water absorbent in the field of adsorption material.

1. Introduction

Exploring highly symmetrical ligands and suitable metal salts to construct supramolecular architectures has attracted much interest [1–4]. Lanthanide coordination frameworks are of great importance currently, not only because of their fascinating architectures but also for their technological applications, such as diagnostic tools, luminescence sensors, absorption, and host–guest chemistry [5–7]. An effective and facile approach in building such networks is to select or design appropriate organic bridging ligands that can bind metal ions in different modes and provide a possible route to achieve more intriguing polymeric structures [8–10]. Carboxylate ligands can be an excellent candidate in supramolecular assembly as a result of its versatile coordination modes [11–13]. So far, great efforts have been devoted to construct the polymers of rare earth (III) salts with rigid aromatic ligands, such as 1,3,5-benzenetricarboxylate [14,15], imidazole-4,5-dicarboxylate [16] and so on. The studies on the metal coordination polymers of H_2L in our lab have confirmed that H_2L is a good building block based on its various conformation and coordination modes [17]. The successful syntheses of these complexes prompted us to further investigate the syntheses and application of lanthanide coordination polymers. Recently, several rare earth polymers with the flexible ligand H_2tzda [H_2tzda=(1,3,4-thiadiazole-2,5-diyldithio)diacetic acid] have been reported by Wang et al. [18–20]. However, complexes with flexible ligand containing carboxylate groups, which exhibit 2-fold interpenetration with intriguing 1D channels, are relatively scarce. In contrast to the rigid ligands, the flexible ones exhibit more conformational and coordination versatility. Furthermore, the resulting structures can be controlled and adjusted through changing their conformation and coordination modes [21]. At present, most of the studies on the complexes have been only confined to description of their synthesis and structure, however, the studies on the application of these complexes as function materials have not drawn enough attention.

Based on above backgrounds, our research interest currently focuses on the construction of novel lanthanide coordination frameworks using the ligand containing carboxylate groups, as well as their application performance in the field of function material. In the present work, the assembly of the ligand H_2L [H_2L=1,2-bis[3-(1,2,4-triazolyl)-4-amino-5-carboxylmethylthio] ethane with lanthanide (III) salts under hydrothermal condition has lead to two coordination polymers with 3D network {$[Ln(L)_{1.5}(H_2O)_2]\cdot 5H_2O$}$n$ [Ln=Y(**1**), Ce(**2**)] containing 2-fold interpenetration. In addition, the reversible desorption–adsorption behavior of lattice water is interestingly found in the two complexes, which is significant because of their potential application as adsorption material in the future.

* Corresponding author. Fax: +86 371 67766017.
E-mail addresses: yt.fan@zzu.edu.cn, yt.fan@371.net, ytfan1207@yahoo.com.cn (Y. Fan).

0022-4596/$ - see front matter © 2010 Elsevier Inc. All rights reserved.
doi:10.1016/j.jssc.2010.07.043

2. Experimental section

2.1. Materials and measurements

All chemicals from commercial sources were of reagent grade and used without further purification. Elemental analyses (C, H, N) were performed on a Carlo-Erba 1160 Elemental analyzer. IR spectra were recorded in the region of 4000–400 cm^{-1} on a Nicolet NEXUS 470-FTIR Spectrophotometer with pressed KBr pellets. UV–Vis absorption spectra in the solid state were taken using a Cary 5000 UV–Vis–NIR spectrophotometer. Themogravimetric analyses were carried out with a NETZSCH STA 409 unit at a heating rate of 10 °C/min under air atmosphere.

2.2. Synthesis of H_2L

1,2-bis[3-(1,2,4-triazolyl)-4-amino-5-mercapto]ethane as starting material was prepared according to the reported procedure [22]. The ligand H_2L was synthesized as follows: (1.89 g, 0.02 mol) chloroacetic acid, 1,2-bis[3-(1,2,4-triazolyl)-4-amino-5-mercapto]ethane (2.58 g, 0.01 mol), sodium carbonate (3.12 g, 0.02 mol), 50 ml water, and refluxed for 3 h under stirring. The mixture was then cooled to room temperature and concentrated hydrochloric acid was introduced with stirring until pH=2. The precipitate was filtered off and washed with water, giving a fine white powder in 64% yield (2.4 g). m.p. 186–187 °C. Anal. Calc. for $C_{10}H_{14}N_8O_4S_2$ (%): C, 32.05; H, 3.74; N, 29.91. Found (%): C, 31.98; H, 3.78; N, 29.94. IR (KBr, cm^{-1}): 3354 (w), 3206 (w), 2930 (w), 1707 (s), 1632 (w), 1428 (m), 1374 (s), 1309 (m), 1229 (m), 1186 (m), 912 (w), 674 (w). 649(w). ^{1}HNMR (400 MHz, DMSO): δ=3.838(s,4H), 3.092(t,4H), 2.075(s,6H); ^{13}C NMR (400 MHz), DMSO): δ=21.54, 31.14, 151.68, 155.79, 170.27 ppm.

2.3. Preparation of {[$Y(L)_{1.5}(H_2O)_2$]·$5H_2O$}n (1)

Polymer **1** is synthesized by the hydrothermal reaction of $Y(NO_3)_3 \cdot 6H_2O$ (1 mmol, 274.9 mg), H_2L (1 mmol, 374 mg), NaOH (2 mmol, 80 mg) and deionized water (14 ml) in a sealed Teflon-lined stainless steel vessel (25 ml) at 120 °C for 7 days. After being cooled to room temperature, crystals of **1** (colorless, block-like) were collected by filtration. Yield: 48% based on Y. Anal. Calc. for $C_{15}H_{32}YN_{12}O_{13}S_3$ (**1**): C, 23.27; H, 4.14; N, 21.72%. Found: C, 23.21; H, 4.18; N, 21.68%. IR data (KBr, cm^{-1}): 3326(m), 1618(w), 1586(s), 1435(s), 1405(s), 1238(m),1029(m), 941(w), 908(w), 777(w), 685(m).

Table 1
Crystallographic data for H_2L and complexes **1** and **2**.

	H_2L	**1**	**2**
Empirical formula	$C_{10}H_{14}N_8O_4S_2$	$C_{15}H_{32}YN_{12}O_{13}S_3$	$C_{15}H_{32}CeN_{12}O_{13}S_3$
M_r	374.41	773.62	824.83
Crystal system	Monoclinic	Triclinic	Triclinic
Space group	$P2_1/c$	$P\bar{1}$	$P\bar{1}$
a (Å)	6.1348(3)	9.4609(19)	9.5879(19)
b (Å)	11.4461(17)	11.458(2)	11.570(2)
c (Å)	11.0712(16)	14.593(3)	14.583(3)
α (deg)	90.000	69.96(3)	69.16(3)
β (deg)	93.133(2)	85.42(3)	85.20(3)
γ (deg)	90.000	86.41(3)	86.30(3)
V (Å^3)	776.3(2)	1480.4(5)	1505.4(5)
Z	2	2	2
μ (mm^{-1})	0.380	2.262	1.800
D_c (g cm^{-3})	1.602	1.736	1.820
F(000)	388	794	832
Goodness-of-fit	1.024	1.018	1.055
R_1 ($I>2\sigma(I)$)	0.0384	0.0601	0.0311
wR_2 (all data)	0.0829	0.1140	0.0847

$R_1=\Sigma||F_o|-|F_c||/\Sigma|F_o|$; $wR_2=[\Sigma w(F_{02}-F_{c2})2/\Sigma w(F_{02})2]1/2$.

2.4. Preparation of {[$Ce(L)_{1.5}(H_2O)_2$]·$5H_2O$}n (2)

The synthesis of **2** was similar to that of **1**, except $Ce(NO_3)_3$ was used instead of $Y(NO_3)_3$ and the reaction time were 5 days. Yield: 51% based on Ce. Anal. Calc. for $C_{15}H_{32}CeN_{12}O_{13}S_3$ (**2**): C, 21.51; H, 3.82; N, 20.08%. Found: C, 21.48; H, 3.85; N, 20.13%. IR data (KBr, cm^{-1}): 3328(m), 1621(w), 1584(s), 1436(s), 1406(s), 1236(m),1029(m), 942(w), 908(w), 777(w), 685(m).

2.5. Single-crystal structure determination

The intensity data for **1** and **2** were collected at 293 K on a Rigaku Saturn 724 CCD diffractometer equipped with graphite-monochromated Mo$K\alpha$ radiation (λ=0.71073 Å). All of the

Table 2
Selected bond lengths (Å) and angles (deg.) for H_2L, complexes **1** and **2**.

H_2L			
S(1)–C(3)	1.7487(14)	O(1)–C(2)	1.2111(19)
S(1)–C(1)	1.8206(16)	O(2)–C(2)	1.3413(18)
*Complex **1***			
Y1–O1	2.305(3)	Y1–O1A	2.684(3)
Y1–O2A	2.394(3)	Y1–O3	2.323(3)
Y1–O4A	2.358(3)	Y1–O5	2.480(3)
Y1–O6	2.528(3)	Y1–O7	2.458(3)
Y1–O8	2.349(3)		
O1–Y1–O3	72.57(10)	O1–Y1–O8	81.55(10)
O3–Y1–O8	132.89(11)	O1–Y1–O4A	76.65(10)
O3–Y1–O4A	134.36(9)	O8–Y1–O4A	72.58(10)
O1–Y1–O2A	122.95(10)	O3–Y1–O2A	84.80(11)
O8–Y1–O2A	141.83(11)	O4A–Y1–O2A	84.15(10)
O1–Y1–O7	145.43(9)	O3–Y1–O7	141.95(10)
O8–Y1–O7	72.91(10)	O4A–Y1–O7	73.75(9)
O2A–Y1–O7	71.52(10)	O1–Y1–O5	100.85(10)
O3–Y1–O5	75.48(9)	O8–Y1–O5	71.58(9)
O4A–Y1–O5	144.03(10)	O2A–Y1–O5	123.41(9)
O7–Y1–O5	92.89(9)	O1–Y1–O6	139.52(10)
O3–Y1–O6	71.64(10)	O8–Y1–O6	110.23(9)
O4A–Y1–O6	143.56(10)	O2A–Y1–O6	71.57(9)
O7–Y1–O6	72.78(9)	O5–Y1–O6	51.95(9)
O1–Y1–O1A	72.39(10)	O3–Y1–O1A	69.28(9)
O8–Y1–O1A	138.01(9)	O4A–Y1–O1A	69.76(9)
O2A–Y1–O1A	50.59(9)	O7–Y1–O1A	112.51(9)
O5–Y1–O1A	144.56(9)	O6–Y1–O1A	111.00(9)
*Complex **2***			
Ce1–O1	2.446(2)	Ce1–O1A	2.650(2)
Ce1–O2A	2.562(3)	Ce1–O3	2.434(2)
Ce1–O4A	2.494(2)	Ce1–O5	2.603(2)
Ce1–O6	2.622(2)	Ce1–O7	2.587(2)
Ce1–O8	2.467(2)		
O1–Ce1–O3	71.33(8)	O1–Ce1–O8	82.67(8)
O3–Ce1–O8	130.59(9)	O1–Ce1–O4A	74.54(8)
O3–Ce1–O4A	134.55(8)	O8–Ce1–O4A	71.84(8)
O1–Ce1–O2A	121.30(8)	O3–Ce1–O2A	87.59(10)
O8–Ce1–O2A	141.38(8)	O4A–Ce1–O2A	85.25(8)
O1–Ce1–O7	144.49(8)	O3–Ce1–O7	143.95(8)
O8–Ce1–O7	73.60(8)	O4A–Ce1–O7	73.18(8)
O2A–Ce1–O7	70.13(8)	O1–Ce1–O5	105.41(8)
O3–Ce1–O5	74.56(8)	O8–Ce1–O5	72.95(8)
O4A–Ce1–O5	144.49(8)	O2A–Ce1–O5	121.01(8)
O7–Ce1–O5	92.61(8)	O1–Ce1–O6	140.53(8)
O3–Ce1–O6	72.18(8)	O8–Ce1–O6	110.84(8)
O4A–Ce1–O6	144.45(8)	O2A–Ce1–O6	71.22(8)
O7–Ce1–O6	73.89(8)	O5–Ce1–O6	81.55(10)
O1–Ce1–O1A	71.69(9)	O3–Ce1–O1A	69.94(8)
O8–Ce1–O1A	139.53(7)	O4A–Ce1–O1A	71.44(8)
O2A–Ce1–O1A	49.62(7)	O6–Ce1–O1A	110.79(8)
O5–Ce1–O1A	143.34(7)	O6–Ce1–O1A	108.84(8)

Symmetry transformations used to generate equivalent atoms: For H_2L: #1 $-x+2$, $-y$, $-z+2$. For **1**: #1 $-x+2$, $-y$, $-z$; #2: $-x+2$, $-y$, $-z+1$; #3: $-x+2$, $-y+1$, $-z+1$; #4: $-x+4$, $-y+1$, $-z$. For **2**: #1 $-x+2$, $-y$, $-z$; #2: $-x+2$, $-y$, $-z+1$; #3: $-x+2$, $-y+1$, $-z+1$; #4: $-x+4$, $-y+1$, $-z$.

structures were solved by direct methods and expanded using Fourier techniques. The non-hydrogen atoms were refined with anisotropic thermal parameters. The hydrogen atoms were assigned with common isotropic displacement factors and included in the final refinement by using geometrical constraints. The final cycle of full-matrix least squares refinement was based on the observed reflections and variable parameters. All calculations were performed using the SHELXL-97 crystallographic software package [23]. Table 1 shows crystallographic data of H_2L and polymers **1** and **2**. Selected bond distances and angles for H_2L and polymers **1** and **2** are listed in Table 2.

3. Results and discussion

3.1. Description of the crystal structures

The crystal structure of the ligand (H_2L) is shown in Fig. 1. The ligand crystallizes in the monoclinic system, space group $P2_1/c$.

Single-crystal X-ray diffraction reveals that title polymers **1** and **2** are isomorphous and isostructural. Hence, only the structure of **1** will be described in detail. Polymer **1** crystallizes in the triclinic system, space group $P\bar{1}$, and the asymmetric unit consists of one Y(III) cation, one and a half L^{2-} anions and two water molecules. Y(III) is nine-coordinated and surrounded by seven oxygen atoms provided by five L^{2-} anions (O1, O1A, O2A, O3, O4A, O5, O6) and two coordination water molecules (O7 and O8) to form a distorted tricapped trigonal prism as depicted in Fig. 2. The Y–O distances range from 2.305(3) to 2.684(3) Å and lie in the range of 2.234(3)–2.878(3) Å which are mostly found for nine-coordinated yttrium cations [24]. In this compound, all carboxyl groups of the H_2L are deprotonated, It should be noted that all the L^{2-} anions in **1** employ three different types of coordination modes (bidentate chelate, bidentate bridging, bidentate chelate bridging) to construct subunits of $[Y_2(L)_3(H_2O)_4]$. L^{2-} anions with bidentate chelate bridging coordination modes link Y(III) centers to form a 1D zigzag chain in *c* direction. The second type of L^{2-} anions with bidentate bridging coordination mode join Y(III) centers to form a 2D layer. The third type of L^{2-} anions which adopt bidentate chelate bridging coordination mode, connect Y(III) centers to form a 3D network, as seen in Fig. 3. Because the single 3D network has spacious voids, it allows one more identical network to interpenetrate giving rise to a 2-fold interpenetrating 3D *a*-polonium network. From a topological view, the formed 3D net of the title polymers can be best described as a doubly interpenetrated six-connected net with the Schläfli symbol of $(4^{12}.6^4)$, as illustrated in Fig. 4, when the $[Y_2(L)_3(H_2O)_4]$ centers are treated as six-connected nodes while L^{2-} anions as bridging linkers.

Interestingly, in **1**, the 3D framework consists of one-dimensional channels along the *b* direction, after the van der Waals radii of the surface atoms are removed, the free channel is sized ca. 12.172 × 18.117 Å. The channels are resided by uncoordinated water molecules (O9, O10, O11, O12, O13), as described in Fig. 5. A series of hydrogen bonds are formed among the coordinated water molecules, the coordinated water and the triazole N atoms, the uncoordinated water and NH_2, respectively, which stabilize the 3D supramolecular architecture. Supposing the lattice water molecules are removed, the hydrogen bond system would be destroyed. For example, the dehydrated example of **1** exhibits a white non-transparent crystal instead of a single crystal form.

3.2. Spectra properties and thermogravimetric analyses

The IR spectra of **1** and **2** show the characteristic absorptions of L^{2-} anions. The absence of band in the region 1690–1730 cm^{-1} indicates the complete deprotonation of the–COOH. The asymmetric

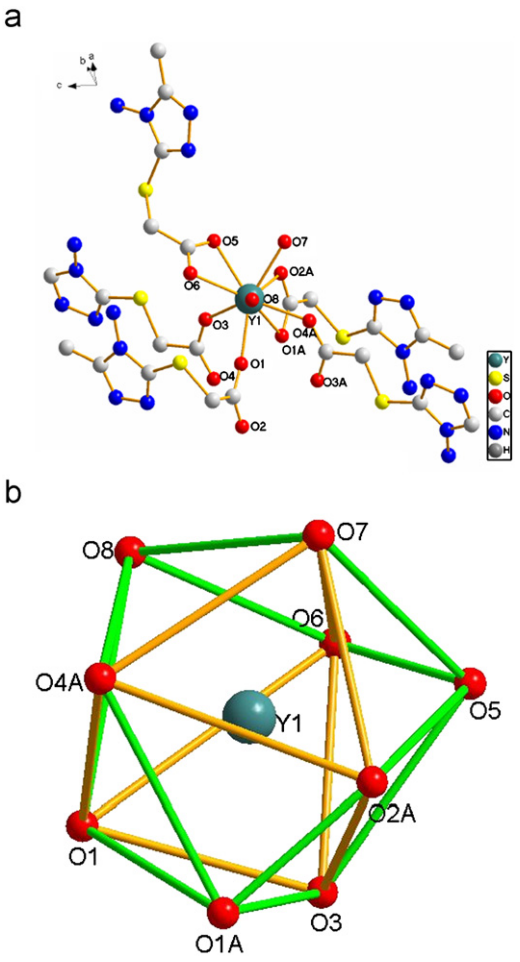

Fig. 2. (a) The coordination environments of Y1 in complex **1** and (b) distorted tricapped trigonal prismatic coordination environment of complex **1** (hydrogen atoms and uncoordinated water molecules were omitted for clarity).

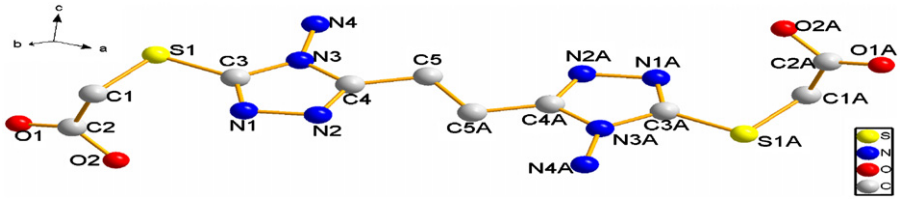

Fig. 1. The molecular structure of H_2L is arranged with atom numberings. Hydrogen atoms have been omitted for clarity.

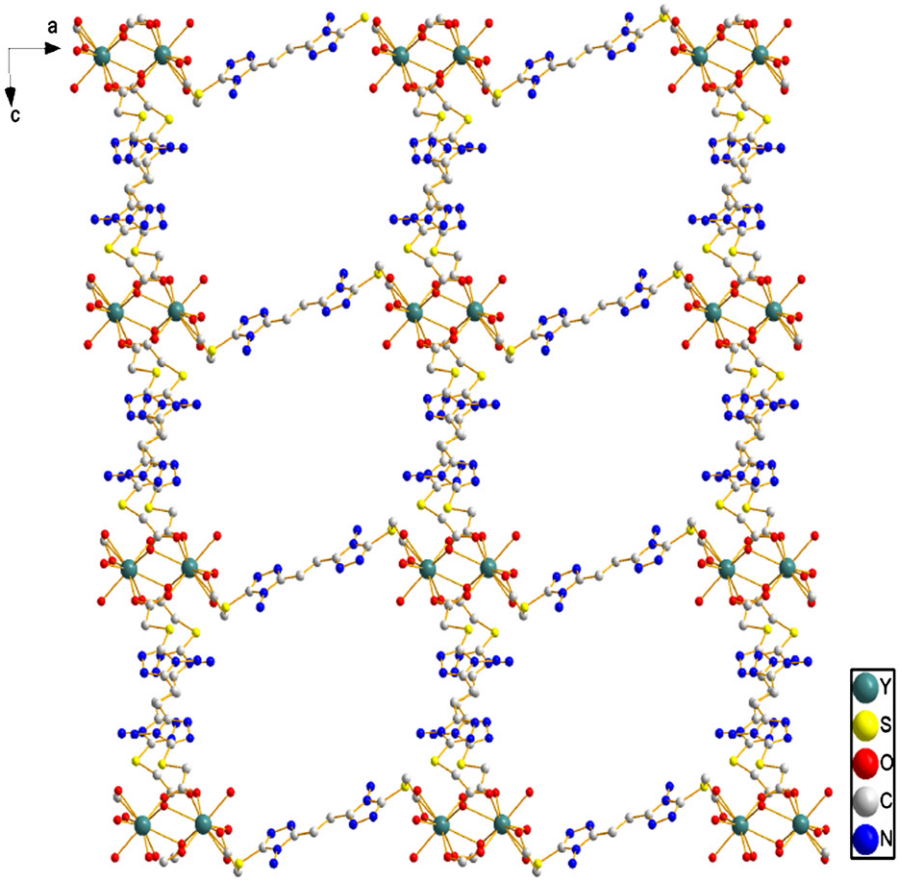

Fig. 3. 3D network of **1** along *b* direction (hydrogen atoms, uncoordinated water molecules are omitted for clarity).

and symmetric stretching vibration bands of–COO^- groups appear at 1618, 1586 and 1405 cm^{-1} for **1**, 1621, 1584 and 1406 cm^{-1} for **2**, respectively, suggesting that–COO^- functions in different coordination modes. The analyses of IR spectra of **1** and **2** are in good agreement with crystal structures and charge balance considerations.

The solid state UV–vis spectra of ligand and the corresponding complexes **1** and **2** are further determined (Fig. S1). The complexes **1** and **2** give similar characteristic absorptions at approximately 240 nm in accord with the free ligand H_2L, which all may be attributed to the intraligand $\pi \rightarrow \pi*$ transition of the ligand. The effective bands at approximately 240 nm for complexes **1** and **2** indicate a slight blue-shift compared to free ligand, presumably due to reduction of the π electron density induced by the coordination of carboxylate group with metal ions.

Thermal stability was measured by TG analysis in air atmosphere. Two samples exhibit similar thermal decomposition behaviors in the range of ambient temperature to 890 °C. They exhibit a good stability at air atmosphere and ambient temperature. The thermal decomposition process of both samples exhibits three main weight losses. The first weight loss of 12.3% happens between 30 and 160 °C for **1** (calcd: 11.6%), which corresponds to the loss of five lattice water. The second loss ranges from 260 to 314 °C, it can be assigned to the loss of the two coordinated water molecules accompanied by the initial breakdown of the organic moieties. Immediately following the third losses start at a temperature above 314 °C which corresponds to the combustion of the organic moieties, and do not end until 800 °C, as demonstrated in Fig. 6a. The final products are not characterized. TGA curve of **2** shows similar thermal decomposition behaviors. The TGA curve exhibits an initial weight loss of 11.8% from 30 to 160 °C for **2** (calcd: 10.9%) (Fig. S2).

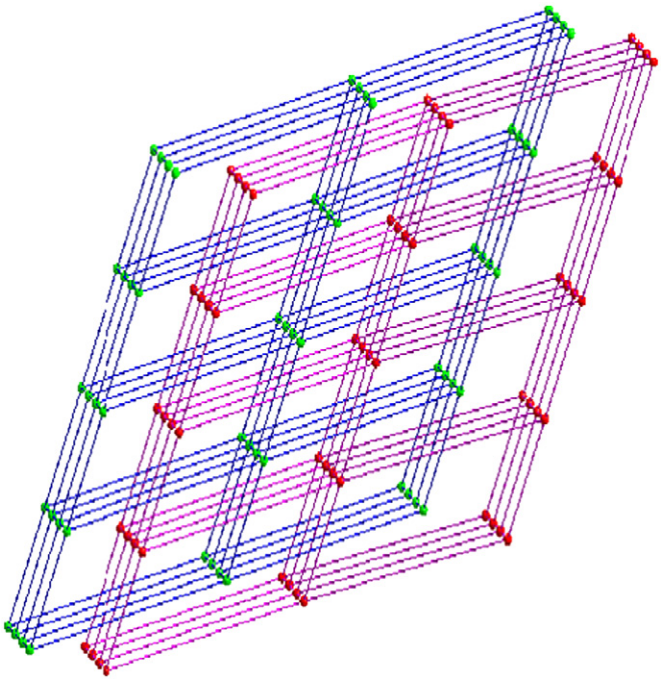

Fig. 4. 1D 2-fold interpenetrating diamondoid nets (circles and straight lines represent Y_2L_3 units and L^{2-} anions, respectively).

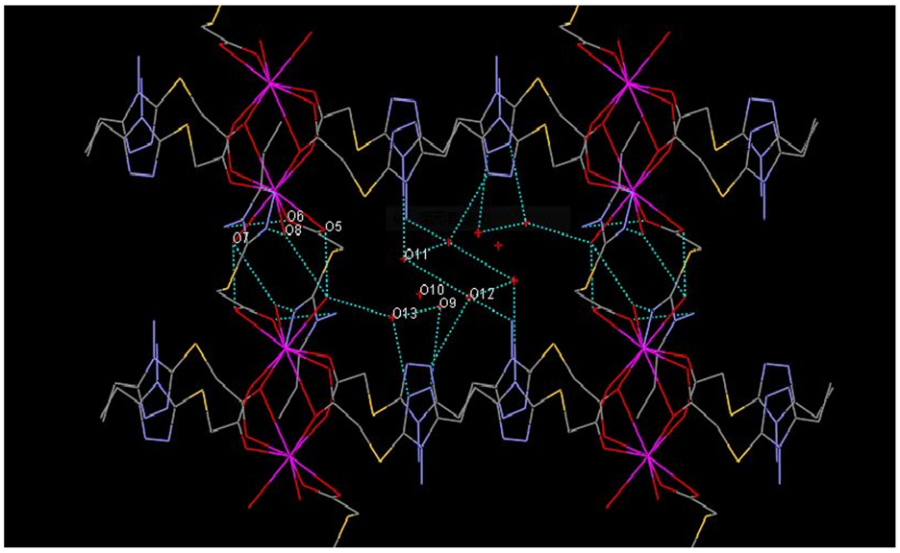

Fig. 5. 3D framework with 1D channels of **1** along *b* direction.

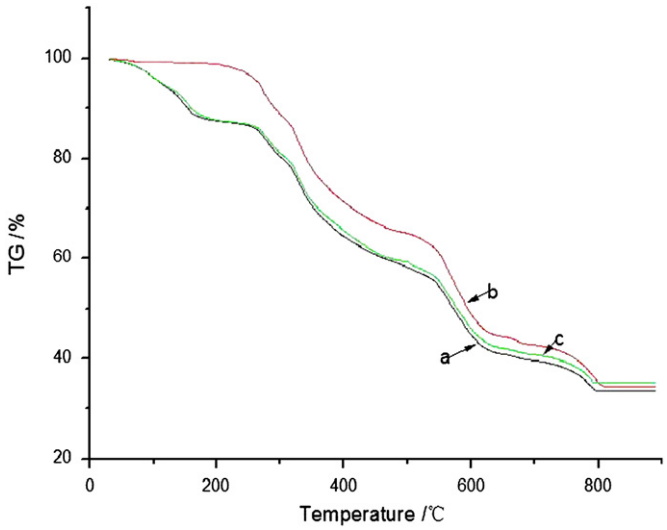

Fig. 6. TG data for complex **1**: (a) as-synthesized sample, (b) dehydrated sample at 160 °C, and (c) rehydrated sample.

3.3. Reversible desorption–adsorption behavior of lattice water

Interestingly, the reversible desorption–adsorption characteristic of lattice water is significantly found in both **1** and **2**. Herein, only the compound **1** will be served as a concrete example to be described in detail. The as-synthesized compound **1** was heated at 160 °C for 12 h in air, and a dehydrated sample was obtained, the predictable chemical composition is $[Y(L)_{1.5}(H_2O)_2]$. as revealed by the elemental analysis experiment (Anal. Calcd: C, 26.33; H, 3.22; N, 24.57%; Found: C, 26.40; H, 3.17 N, 24.63%). The results of elemental analyses show that five lattice water molecules in the compound **1** are fully desorbed, but two coordination water molecules in the compound **1** still maintained. This result is consistent with thermal analysis data as illustrated in Fig. 6b. However, the dehydrated example exhibits a white non-transparent crystal instead of a single crystal form (Fig. 7-2). Interestingly, the dehydrated example of $[Y(L)_{1.5}(H_2O)_2]$ can be restored to the single crystal form of $[Y(L)_{1.5}(H_2O)_2]\cdot 5H_2O$ again after being soaked in water for 2 days, as shown by the elemental analysis experiment (Anal. Calcd: C, 23.27; H, 4.14; N, 21.72%. Found: C, 23.23; H, 4.16; N, 21.67%). The prediction is further verified by the thermal analysis (Fig. 6c) and XRD (Fig. 7-4d) legend. The rehydrated example exhibits the same characteristic diffraction peaks in XRD patterns (Fig. 7-4d) compared with that of the compound **1** (Fig. 7-4b). Furthermore, the similar crystallographic data of the restored sample based on the compound **1** are also obtained by single-crystal X-ray diffraction analysis. Hence, the desorption–adsorption characteristic of lattice water in the compound **1** is a reversible process in our tests. Similar phenomenon is also observed in compound **2** (Fig. S2).

The phenomenon can be explained, according to Kitagawa classification, the reversible desorption–adsorption behavior of lattice water may be attributed to the guest-induced crystal-to-crystal transformation in the framework of compounds **1** and **2** [25]. Meantime, the 3-D framework in the compound has not been destroyed and the close-packing force is effective when the guest water molecules are removed, and the single crystal form of $[Ln(L)_{1.5}(H_2O)_2]\cdot 5H_2O$ is restored again with the reintroduction of water molecules. It is not difficult to understand owing to hydrogen bond-regulated microporous nature within the compound structure [26,27]. Recently, an analogue illustration based on complex $[Tb_2(BDOA)_3(H_2O)_4]\cdot 6H_2O$ is reported by Hong et al. [28], in which the crystal form of $[Tb_2(BDOA)_3(H_2O)_4]\cdot 6H_2O$ can be converted into the amorphous powder of $[Tb_2(BDOA)_3(H_2O)_2]$ by heating at 120 °C for 12 h, and then the latter is restored to the crystalline form of $[Tb_2(BDOA)_3(H_2O)_4]\cdot 6H_2O$ after being soaked in water for 12 h. However, two coordination water molecules in $[Tb_2(BDOA)_3(H_2O)_4]\cdot 6H_2O$ are simultaneously removed with the desorption of lattice water in the first dehydration stage, meanwhile, a low dehydrated temperature of 120 °C is observed in the complex. As can be seen from the above results, the thermal stability based on the dehydration temperature of crystal water for $[Tb_2(BDOA)_3(H_2O)_4]\cdot 6H_2O$ is not very well as compared with that of the title two compounds. Furthermore, the rate of water content for **1** is about 13.2% (w/w) while the latter is about 12.3% (w/w). The above results imply that the title two compounds may be used for late-model desiccant/water absorbent as potential adsorption material.

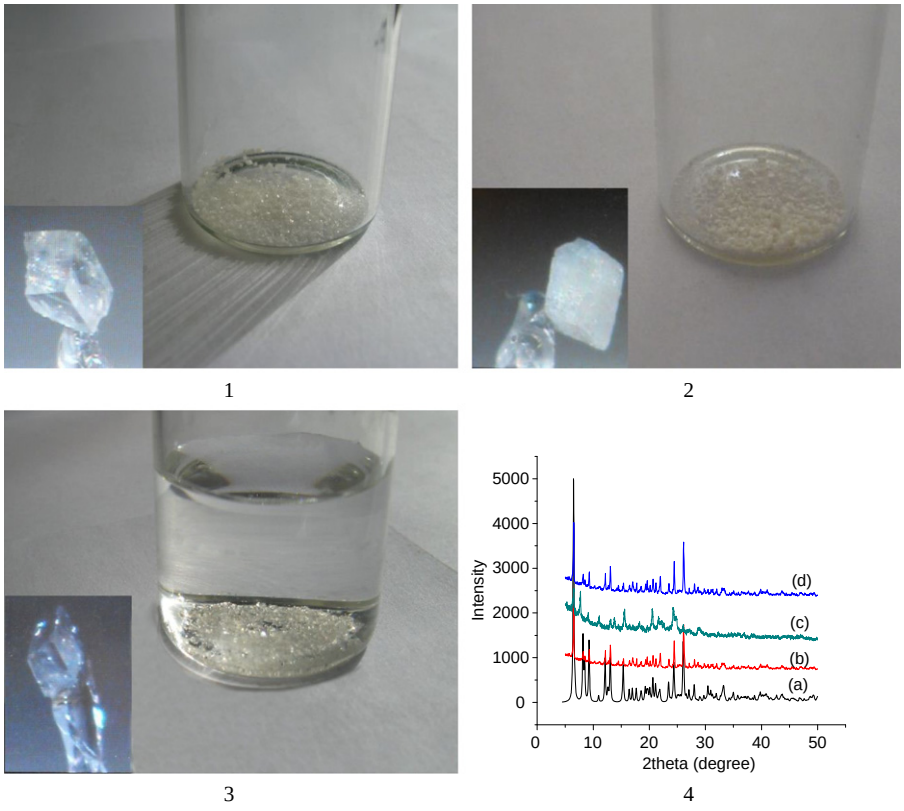

Fig. 7. (1) Images of as-prepared complex **1** and its' single crystal photo; (2) images of dehydrated products of complex 1 and its' amorphous solid photo; (3) images of rehydrated products of complex **1** and its' single crystal picture; (4) PXRD patterns: (a) simulated pattern of complex **1**; (b) as-prepared complex **1**; (c) dehydrated products of complex **1**; and (d) rehydrated products of complex **1**.

4. Conclusions

Two novel 3D network lanthanide (III) complexes containing 2-fold interpenetration, $\{[Ln(L)_{1.5}(H_2O)_2]\cdot 5H_2O\}n$[$Ln$=Y(**1**), Ce(**2**); L=1,2-bis[3-(1,2,4-triazolyl)-4-amino-5-carboxylmethylthio] ethane have been obtained. The reversible desorption–adsorption behavior of lattice water for the title compounds has been investigated. The results indicate that they may be good candidate as late-model desiccant/water absorbent in the field of adsorption material.

Acknowledgment

The authors gratefully acknowledge the financial support from the National Natural Science Foundation of China (nos. 20871106 and 91010008).

Appendix A. Supplementary data

CCDC nos. 747782, 747783 and 747784 contains the supplementary crystallographic data for this paper. These data can be obtained free of charge from the Cambridge Crystallographic Data Centre, 12, Union Road, Cambridge CB2 1EZ, UK; fax: +44 1223 336033.

Appendix B. Supporting information

Supplementary data associated with this article can be found in the online version at doi:10.1016/j.jssc.2010.07.043.

References

[1] S. Ma, H.C. Zhou, J. Am. Chem. Soc. 128 (2006) 11734.
[2] K.C. Hee, K. Jaheon, D.F. Olaf, O. Michael, M.Y. Omar, Angew. Chem. Int. Ed. 42 (2003) 3907.
[3] C.J. Kepert, M.J. Rosseinsky, Chem. Commun. (1999) 375.
[4] S.N. Wang, H. Xing, Y.Z. Li, J.F. Bai, Y. Pan, M. Scheer, X.Z. You, Eur. J. Inorg. Chem. 15 (2006) 3041.
[5] (a) D. Parker, Coord. Chem. Rev. 205 (2000) 109;
(b) K. Kuriki, Y. Koike, Chem. Rev. 102 (2002) 2347;
(c) J. Kido, Y. Okamoto, Chem. Rev. 102 (2002) 2357;
(d) G.Y. Adachi, N. Imanaka, S.J. Tamura, Chem. Rev. 102 (2002) 2405.
[6] M.L. Tong, X.M. Chen, S.R. Batten, J. Am. Chem. Soc. 125 (2003) 16170–16171.
[7] W.P. Su, M.C. Hong, J.B. Weng, R. Cao, S.F. Lu, Angew. Chem. Int. Ed. 39 (2000) 2911–2914.
[8] I.M. Müller, R. Robson, Angew. Chem. Int. Ed. 39 (2000) 4357.
[9] B.F. Abrahams, P.A. Jackson, R. Robson, Angew. Chem. Int. Ed. 37 (1998) 2656.
[10] H.W. Roesky, M. Andruh, Coord. Chem. Rev. 236 (2003) 91.
[11] A. Distler, S.C. Sevov, Chem. Commun. 8 (1998) 959.
[12] N. Barooah, R.J. Sarma, A.S. Batsanov, J.B. Baruah, Polyhedron 25 (2006) 17.
[13] C.A. Schalley, A. Lützen, M. Albrecht, Chem. Eur. J. 10 (2004) 1072.
[14] S.S.Y. Chui, S.M.F. Lo, J.P.H. Charmant, A.G. Orpen, I.D. Williams, Science 283 (1999)1148 283 (1999).
[15] N.L. Rosi, M. Eddaoudi, J. Kim, M. O'Keeffe, Angew. Chem. Int. Ed. 41 (2002) 284.
[16] W.G. Lu, C.Y. Su, T.B. Lu, L. Jiang, X.M. Chen, J. Am. Chem. Soc. 128 (2006) 34.
[17] W.J. Chu, X.W. Hou, Q.H. Zhao, Y.T. Fan, H.W. Hou, Inorg. Chem. Commun. 13 (2010) 22.
[18] Y.T. Wang, L.P. Zhang, Y.T. Fan, H.W. Hou, X.Q. Shen, Inorg. Chim. Acta 360 (2007) 2958.
[19] Y.T. Wang, X.Q. Shen, Y.T. Fan, H.C. Yao, H.W. Hou, Supramol. Chem. 2 (2008) 501.
[20] Y.T. Wang, Y. Xu, Y.T. Fan, H.W. Hou, J. Solid State Chem. 182 (2009) 2707.
[21] G. Wu, X.F. Wang, T. Okama, W.Y. Sun, N. Ueyama, Inorg. Chem. 45 (2006) 8543.
[22] P.F. Xu, X.W. Sun, L.M. Zhang, Z.Y. Zhang, J. Chem. Res. (S) (1999) 170.

[23] G.M. Sheldrick, in: SHELXL-97, Program for the Solution and Refinement of Crystal Structures, University of Göttingen, Göttingen, Germany, 1997.
[24] Y. Huang, B. Yan, M. Shao, Z.Y. Zhang, J. Solid State Chem. 182 (2009) 657.
[25] S. Kitagawa, R. Kitaura, S. Noro, Angew. Chem. Int. Ed. 43 (2004) 2334.
[26] A.J. Blake, S.J. Hill, P. Hubberstey, W.S. Li, J. Chem. Soc. Dalton Trans. (2004) 913–914.
[27] D. Li, K. Kaneko, Chem. Phys. Lett. 335 (2001) 50–56.
[28] X.L. Hong, Y.Z. Li, H.M. Hu, Y. Pan, J.F. Bai, X.Z. You, Cryst. Growth Des. 6 (2006) 1221–1226.